

Comparative energy analysis of hydrogen carriers as energy source on ships

van Rheenen, Erin S.; Padding, Johan T.; Kana, Austin A.; Visser, Klaas

10.1080/20464177.2024.2448057

Publication date

Document Version Final published version

Published in

Journal of Marine Engineering and Technology

Citation (APA)

van Rheenen, E. S., Padding, J. T., Kana, A. A., & Visser, K. (2025). Comparative energy analysis of hydrogen carriers as energy source on ships. *Journal of Marine Engineering and Technology*. https://doi.org/10.1080/20464177.2024.2448057

Important note

To cite this publication, please use the final published version (if applicable). Please check the document version above.

Other than for strictly personal use, it is not permitted to download, forward or distribute the text or part of it, without the consent of the author(s) and/or copyright holder(s), unless the work is under an open content license such as Creative Commons.

Takedown policy

Please contact us and provide details if you believe this document breaches copyrights. We will remove access to the work immediately and investigate your claim.



Journal of Marine Engineering & Technology



ISSN: (Print) (Online) Journal homepage: www.tandfonline.com/journals/tmar20

Comparative energy analysis of hydrogen carriers as energy source on ships

Erin S. van Rheenen, Johan T. Padding, Austin A. Kana & Klaas Visser

To cite this article: Erin S. van Rheenen, Johan T. Padding, Austin A. Kana & Klaas Visser (09 Jan 2025): Comparative energy analysis of hydrogen carriers as energy source on ships, Journal of Marine Engineering & Technology, DOI: 10.1080/20464177.2024.2448057

To link to this article: https://doi.org/10.1080/20464177.2024.2448057

9	© 2025 The Author(s). Published by Informa UK Limited, trading as Taylor & Francis Group.
	Published online: 09 Jan 2025.
	Submit your article to this journal 🗹
hh	Article views: 112
Q ^L	View related articles 🗗
CrossMark	View Crossmark data ☑







Comparative energy analysis of hydrogen carriers as energy source on ships

Erin S. van Rheenen [©]a, Johan T. Padding^b, Austin A. Kana^a and Klaas Visser^a

^aDepartment of Maritime and Transport Technology, Delft University of Technology, Delft, The Netherlands; ^bDepartment of Process and Energy, Delft University of Technology, Delft, The Netherlands

ABSTRACT

Hydrogen carriers are attractive alternative fuels for the shipping sector. They are zero-emission, have high energy densities, and are safe, available, and easy to handle. Sodium borohydride, potassium borohydride, dibenzyltoluene, n-ethylcarbazole, and ammoniaborane are hydrogen carriers with high theoretical energy densities. The energy density is paramount to implementing hydrogen carriers as a high energy density enables compact and lightweight storage. The effective energy density depends on integrating heat and masses with energy converters. This combination defines the energy efficiency and, thus, the energy density of the system. This paper addresses the effective energy density of the hydrogen carriers, including the dehydrogenation process. Using a 0D model, we combined the five carriers with two types of fuel cells, namely proton exchange membrane (PEM) and solid oxide fuel cells (SOFC), an internal combustion engine and a gas turbine. N-ethylcarbazole and dibenzyltoluene offer medium energy densities, reaching almost 4 MJ/kg. However, the effective energy density of sodium borohydride and ammoniaborane is very high, up to 15 MJ/kg, including the energy converter. This is similar to the energy density of marine diesel oil combined with an internal combustion engine. Thus, we conclude hydrogen carriers are alternative fuels that deserve more attention because of their strong potential to make shipping zero-emission.

ARTICLE HISTORY

Received 28 March 2024 Accepted 24 December 2024

KEYWORDS

Alternative fuel; energy analysis; hydrogen carrier; hydrogen generation

1. Introduction

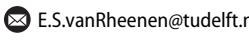
The shipping sector, which uses oil-based fuels, emits 3% of global greenhouse gases (International Energy Agency 2021). The sector is not on track to reach net-zero greenhouse gas emissions by 2050 (International Energy Agency 2021; IMO 2023). Alternative low- and zero-carbon fuels, such as ammonia, methanol, LNG and hydrogen, are considered convenient alternative fuels to reduce greenhouse gases (Kass et al. 2021). The diversity of ship types makes it impossible for a single alternative fuel to meet all their current requirements. Ammonia and methanol are toxic. Methanol and LNG still emit CO₂ and other harmful emissions, and LNG is a fossil fuel, making it unsustainable. Gaseous hydrogen has a low volumetric energy density, and pure hydrogen is extremely flammable. However, hydrogen is the only fuel with local zero green house gas emission performance as it theoretically emits only water when used, with possible NO_x emissions if combusted. The major issues with hydrogen, the low energy density and high flammability, can be resolved by storing hydrogen in hydrogen carriers.

Hydrogen carriers are liquid or solid substances that can store and release hydrogen when required. They store hydrogen by chemically bonding it or adsorbing it into their structure. Thus, very little (in the order of at most a few litres as buffer and in pipelines) hydrogen gas is present onboard. In previous research, we have looked into detail in hydrogen carriers and their possible usage on ships (Van Rheenen et al. 2023). During this research, methanol was disregarded as it is not locally CO2 neutral, even though it can be theoretically carbon neutral, as CO₂ capture on ships is not a viable option yet (Van Hoecke et al. 2021). Additionally, methanol is often used as a direct fuel, not as a hydrogen carrier in the sense that hydrogen is extracted. Ammonia is not regarded because of its high toxicity. The hydrogen carriers we identified are generally safer than ammonia, cryogenic and compressed hydrogen and are believed to deliver energy densities that are sufficiently high to meet the required standards. The as promising identified hydrogen carriers are the following: two liquid organic hydrogen carriers (LOHCs): N-ethylcarbazole (NEC) and dibenzyltoluene (DBT), and three boron-based carriers: sodium borohydride (SB, NaBH₄), potassium borohydride (PB, KBH₄), and ammonia borane (AB, NH3BH3) (Van Rheenen et al. 2023). However, we only evaluated whether these hydrogen carriers comply with the theoretical requirements. In reality, the energy density of these hydrogen carriers depends on much more than just the theoretical energy density. Examples include packing factors, different densities depending on particle size and energy loss in the dehydrogenation process. Most research focuses only on LOHCs combined with fuel cells and is not in a maritime context, such as but not limited to (Li et al. 2023; Lee et al. 2021; Preuster et al. 2018; Niermann et al. 2019; Müller et al. 2019). Only very few studies looked at hydrogen carriers integrated as mentioned here (LOHCs, boron-based carriers, but also metal organic frameworks) on ships, not always including calculations (Düll et al. 2022; Van Hoecke et al. 2021; Wu et al. 2023; Otto et al. 2022; Santos 2022). None of these studies include thorough calculations on a multitude of hydrogen carriers on ships.

This study aims to obtain the effective energy density values of the previously identified hydrogen carriers, including the dehydrogenation process. Effective energy density is defined here as the amount of energy that can be transferred to a ship's propulsion system per unit weight of a hydrogen carrier. This definition takes into account the following factors:

- Additional tank weight (when applicable)
- The practical energy required for hydrogen release

CD Delft, The Netherlands



CONTACT Erin S. van Rheenen 🔯 E.S.vanRheenen@tudelft.nl 🔁 Department of Maritime and Transport Technology, Delft University of Technology, Mekelweg 2, 2628

In essence, the effective energy density represents how much energy 1 kg of a hydrogen carrier can deliver to the ship's propulsion. Therefore, it must include the weight of the storage tank and the energy needed for hydrogen release. The latter can be optimized by capturing and utilising waste energy from the energy conversion system (such as an engine or fuel cell). Our study will utilise a zero-dimension (0D) integration model of the five aforementioned hydrogen carriers combined with four different energy converters to find the efficiency of the combinations. The effective energy density of the different hydrogen carrier and energy converter combinations follows from this efficiency. This contribution will give insight into which hydrogen carriers should be considered alternative fuels in the maritime industry.

2. Selection of hydrogen carriers and energy converters

We consider five different hydrogen carriers: two LOHCs (DBT and NEC), two borohydrides (sodium borohydride and potassium borohydride) and ammonia borane. These hydrogen carriers have a medium to high theoretical energy density, are generally considered safe and have a medium to high technology readiness level. Additionally, they do not require temperatures above approximately 573 K, offering possibilities to extract heat from the flue gasses. The processes neither require high pressures for their dehydrogenation process. Furthermore, the dehydrogenation process releases all the hydrogen inside the molecule, and the hydrogen carriers are wellresearched, resulting in enough information to look further into the integration process. Table 1 gives an overview of the hydrogen carriers and their theoretical energy densities when used onboard ships. The energy converter is the machine that converts the chemical energy in hydrogen into either electrical or mechanical energy. Additionally, it also influences the hydrogen carrier's overall energy density. Integrating the waste heat of the energy converter with the dehydrogenation process may reduce significant energy losses (Lee et al. 2021). Four different types of energy converters are considered. On the one hand, we look at conventionally used energy converters such as internal combustion engines (ICE) and gas turbines (GT) and on the other hand, at innovative technologies like fuel cells, specifically solid oxide fuel cells (SOFC) and proton exchange membrane fuel cells (PEMFC).

2.1. Hydrogen carriers

In this section, we will give a concise description of the used hydrogen carriers and the specific properties needed to calculate the overall efficiency of a hydrogen carrier-energy converter system, such as the energy required for dehydrogenation. For a more thorough description of hydrogen carriers and more detailed selection criteria, we refer to Van Rheenen et al. (2023). The specified hydrogen carriers are split into two categories to analyse hydrogen carriers using a 0D thermodynamic model: an exothermic and endothermic type, as this model focuses on heat, mass and processes. Hydrogen carriers

Table 1. Theoretical volumetric and gravimetric energy densities of hydrogen carriers for explicit application onboard ships based on the lower heating value of the hydrogen released (Van Rheenen et al. 2023; Aronietis et al. 2016).

Carrier	MJ/kg	MJ/L
Ammonia borane	23.52	14.4
SB (hydrolysis)	25.56	27.34
PB (hydrolysis)	17.76	20.78
LOHC: DBT	7.44	7.0
LOHC: NEC	6.98	6.63
MDO	39	41

that release hydrogen endothermically, absorb heat when releasing hydrogen and form a heat sink. On the other hand, hydrogen carriers that release hydrogen exothermically, release heat during the hydrogen release process. These carriers form a heat source. LOHCs release hydrogen endothermically, while boron-based carriers have an exothermic release process (Van Rheenen et al. 2023).

2.1.1. LOHCs

DBT and NEC are chosen because DBT has one of the highest energy densities of LOHCs and NEC has a relatively low release temperature. LOHCs release hydrogen endothermically at elevated temperatures. Equation (1) shows the general release mechanism of LOHCs.

$$LOHC^{+} + Heat \rightarrow LOHC^{-} + nH_{2}$$
 (1)

The exact release temperature depends on the LOHC and the corresponding catalyst. For DBT, the temperatures lie between 553 and 593 K; for NEC, the temperatures lie between 453 and 523 K (Niermann et al. 2019). The dehydrogenation and decomposition temperatures of DBT are similar, requiring careful heat control and possible gaseous stream cleanup. Additionally, external heat may be required for complete dehydrogenation. NEC has better dehydrogenation kinetics in general (Niermann et al. 2019; Peters et al. 2016). However, its spent fuel is solid at room temperature, requiring continuous heating until it enters the tank, and its overall energy density is lower.

2.1.2. Borohydrides and ammonia borane

Ammonia borane, sodium borohydride, and potassium borohydride are solid powders with similar chemical properties at ambient conditions, including a high theoretical density and hydrogen release through hydrolysis. The release of hydrogen through hydrolysis with the borohydrides (sodium borohydride and potassium borohydride) is very similar, taking the example of sodium borohydride:

$$NaBH_4 + (2 + x)H_2O \rightarrow 4H_2 + NaBO_2.xH_2O + Heat$$
 (2)

In this reaction, x stands for a number, as sodium metaborate hydrate is likely formed (Andrieux et al. 2012). The reaction is exothermic; energy is released during the dehydrogenation process, thus requiring cooling. A drawback of borohydrides is that the spent fuel is heavier than the original fuel. The amount of water molecules bonded and, thus, the weight of the spent fuel depends on the reaction process and the temperature of the process. The dehydrogenation process in this research is set to occur at 353 K. The x in NaBO₂.xH₂O depends on the temperature and the amount of water available in the mixture. Andrieux et al. (2012) gives an overview of the exact composition. Without crystallisation, the x will be 2. After crystallisation, x will become 1/3 (Andrieux et al. 2012). Potassium borohydride has a similar reaction equation, including a similar spent fuel: $KBO_2.xH_2O$. However, the x has a lower value for potassium borohydride. At 353 K, x equals 4/3. This stays the same when all water is removed (Krol et al. 2009; Bonnetot and Laversenne 2005).

The dehydrogenation mechanism of ammonia borane is similar, although it forms different products. Equation (3) describes the dehydrogenation reaction. The spent fuel of ammonia borane is independent of temperature and amount of water.

$$NH_3BH_3 + 3H_2O \rightarrow 3H_2 + B(OH)_3 + NH_3 + Heat$$
 (3)

However, the hydrolysis reaction produces the toxic gas ammonia next to the metaborate. This gas can either be burned in a heat engine, decomposed into N2 and H2 for use in a fuel cell or stored on board. The final option is considered impractical for ships because

it requires a completely different, additional storage system, significantly reducing the energy density of the system. This study disregards the second option (cracking) due to its complexity and additional space requirements. Thus, in this study, we will work with the resulting mixture of H₂ and NH₃ as input fuel for the energy converters when using ammonia borane.

2.2. Energy converters

Energy converters are devices that convert chemical energy into electrical or mechanical energy. Ships typically use compression ignition ICEs, but these have challenges when using hydrogen as a single fuel due to its high auto-ignition temperature (Dimitriou and Tsujimura 2017). Additionally, the (mitigation of the) risk of NO_x production in internal combustion engines is a vital attention point. Thus, the sector is considering alternative energy converters, such as spark ignition ICE and fuel cells. We have identified four promising energy converters for the maritime sector: spark ignition ICEs, gas turbines, PEMFCs and SOFCs. Spark ignition ICEs are similar to current engines, while GTs have been used on ships before due to their high power density (Fatsis 2022). Both can, in theory, be run on alternative fuels such as hydrogen, and their high outlet temperatures make them suitable for heat integration. Fuel cells have gained attention because of their modularity and high efficiency. PEMFCs are low-temperature fuel cells that require pure hydrogen, whereas SOFCs operate at much higher temperatures and are less sensitive to poisoning. Both have high efficiencies but only produce electricity, so an electrical drive system is required.

3. Method

To assess the efficiency and, thus, the total energy density of the hydrogen carrier, we constructed a simplified 0D thermodynamic model. The electricity or mechanical energy produced in the energy converter is not converted to the same energy output to ensure a fair and balanced comparison. Each energy converter converts energy most efficiently.

Additionally, the required mass of additional water for sodium borohydride and potassium borohydride are evaluated, as these might significantly influence the comparison of these fuels.

3.1. Special considerations regarding sodium borohydride and potassium borohydride

Sodium borohydride and potassium borohydride are similar substances in almost all respects except for the theoretical energy density, spent fuel composition and water requirements. The theoretical energy density of potassium borohydride is significantly worse than that of sodium borohydride (Van Rheenen et al. 2023). Storage and handling conditions are supposed to be easier for potassium borohydride (Bonnetot and Laversenne 2005; Düll et al. 2022). Its spent fuel is also less susceptible to crystallisation than NaBO₂. Yet, the latter is not necessarily an advantage, as crystallisation is necessary to increase the energy density. Without crystallisation, the spent fuel would hold large amounts of water and thus be heavier and require more space than necessary. However, crystallization does cost additional heat and energy. Furthermore, a separate crystallizer has to be added onboard, increasing overall system size and complexity. Finally, drying the spent fuel changes the product and is likely to influence the handling of the product.

The dehydrogenation process of potassium borohydride requires less water. Thus, with an imperfect water recovery system, potassium borohydride may be superior to sodium borohydride, as no extra water would be necessary. Therefore, this will be checked to see whether potassium borohydride has a real advantage over sodium borohydride or if it is worse or equal in all perspectives. As ammonia borane also requires water, it is also included in this small model.

Despite the easy access to water onboard ships, less water requirements during the dehydrogenation process may be an advantage. The water required for hydrolysis has to be pure water, which is usually acquired using reverse-osmosis pumps. A closed water loop would thus result in less pumping power being required.

The stoichiometric hydrolysis equations are used to calculate the water requirements of the boron-based hydrogen carriers. The stoichiometric equation for ammonia borane can be seen in Equation (3). Stochiometric relations for the borohydrides are as follows (Bonnetot and Laversenne 2005):

$$NaBH_4 + 4H_2O \rightarrow 4H_2 + NaBO_2.2H_2O$$
 (4)

$$KBH_4 + 10/3H_2O \rightarrow 4H_2 + KBO_2.4/3H_2O$$
 (5)

Additionally, the water that becomes available after the energy converter is calculated according to the following equation:

$$2H_2 + O_2 \rightarrow 2H_2O \tag{6}$$

A small model compares the overall water required with the water available from the energy converters. As not all water may be usable, a range of usable water is set, ranging from 50% to 100%, with 100% meaning that all water acquired from the burning or reaction of hydrogen can be used.

3.1.1. Water recovery potential

The potential of water recovery from the outlet largely depends on whether the water is in fluid or in gas phase. If the water is in gas phase, as water vapour, a water separator is limited by the fact that it cannot tamper with the outlet. For example, a water separator behind a hydrogen internal combustion engine could recover at most 50% of the available water, to avoid tampering with the outlet (Yamada and Mohamad 2010). As the gas turbine operates at higher temperatures, it is assumed that a water separator will have a similar efficiency.

SOFCs also have higher operating temperatures, resulting in an outlet of steam. However, SOFCs also have anode off-gas recirculation loops, where steam is condensed from the exhaust gas (Peters et al. 2016). This helps maintain a stable hydrogen-to-steam ratio in the fuel cell and lowers the total gas flow through the system (Peters et al. 2016). This in turn influences the system efficiency. Thus, removing this water from the SOFC system to use in other systems may influence the overall system efficiency of the SOFC.

PEMFCs have a much lower outlet temperature. Calculations by Yao et al. (2022) show that efficiencies of up to 110% can be achieved with simple water recovery at slightly elevated pressures of 4 atm. With expanded water recovery, efficiencies of up to 180 % (at 4 atm) can be reached, while at 1 atm, efficiencies over 100% can be achieved as well (Yao et al. 2022).

Thus, no additional water is required when using a PEMFC, but for the other three energy converters, the water recirculation rate is likely lower than 100% and comparing the additional water requirements is relevant.

3.2. 0D thermodynamic model

Thisresearch makes use of a 0D thermodynamic model. In this model, mass and heat are calculated and compared. Figure 1 gives an overview of the model. The model's input is formed by setting an energy requirement and choosing a hydrogen carrier and an energy converter. The model then estimates the mass of the hydrogen carrier based on previous calculations. This hydrogen carrier mass goes

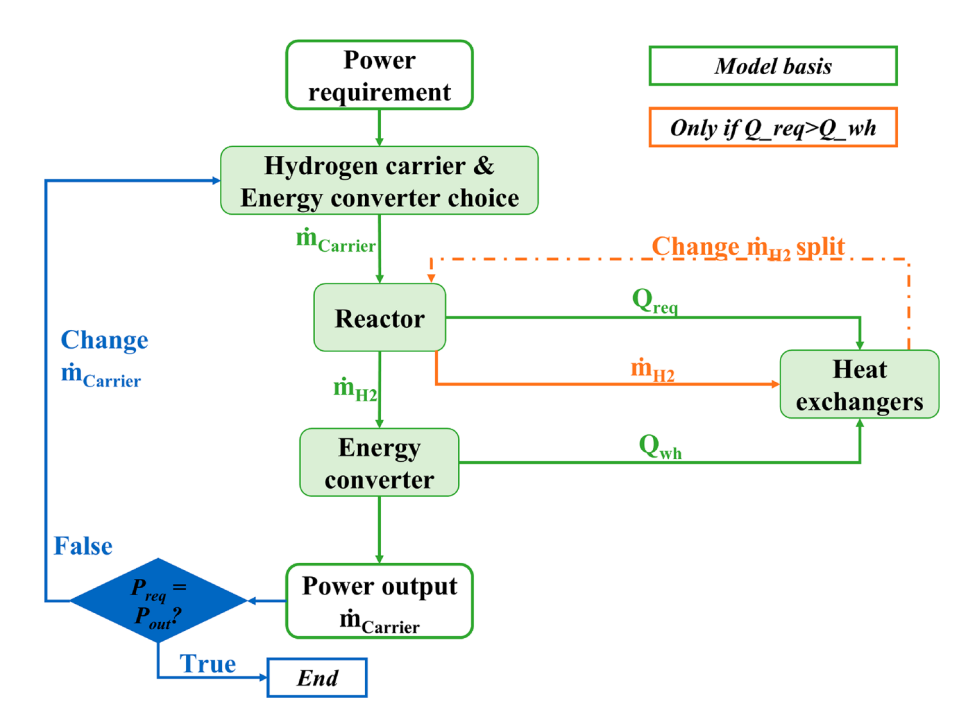


Figure 1. Representation of the 0D thermodynamic model.

into the reactor, where it is split into spent fuel and hydrogen. The hydrogen goes to the energy converter. Next to the spent fuel and the mass, there will be a heating requirement for the reactor to operate. This heating requirement consists of the preheating and dehydrogenation heat (the latter only if the heating requirement is positive). The preheating is calculated using the following equation:

$$Q = m \cdot c_{p,avg} \cdot \Delta T \tag{7}$$

with Q the heat required or released (if the temperature difference is negative) in kJ, m the complete mass of the hydrogen carrier (in the case of the borohydrides including the water) in kg, $c_{p,avg}$ the heat capacity of the overall fluid in kJ/kgK and ΔT the temperature difference in Kelvin. The heat requirement is sent to the heat exchangers, which are assumed to be 100% efficient.

The hydrogen carrier and energy converter choice also defines the resulting hydrogen mass. This hydrogen mass goes to the energy converter, where the parameters from Table 2 are used to calculate the energy output (E_{out}) , waste heat (Q_{wh}) , and irrecoverable losses.

In the heat exchanger, the available waste heat and corresponding temperatures are compared to the required heat and its corresponding temperatures. Figure 2 illustrates the heat flows calculated in the model. These heat flows correspond to different processes, but not all of them are applicable in every scenario. Each heat flow is associated with a specific heat exchanger (HEX), each of which is labelled

Table 2. Parameters of energy converters, parameters adapted from (Wang et al. 2019; Zhao et al. 2017; van Veldhuizen et al. 2023; Gohary and Seddiek 2013; Rosado et al. 2019).

Parameter	SI-ICE	PEMFC	SOFC	GT
P effective [%]	35	42.9	48	37.5
T coolant [K]	363	348	_	_
P coolant [%]	30	44.8	0	0
T flue gas [K]	623*	_	1023	790
P flue gas [%]	25	0	42.1	53.5
P losses [%]	10	12.3	9.9	9.5

With P percentages of overall power distribution, mainly based on Sankey diagrams. *Flue gas temperature of H-2-ICE largely fluctuates depending on operating conditions and can range from 423 to 773 K

(e.g. HEX1, HEX2, HEX3.1). The figure provides a detailed layout of the heat exchanger configuration and their roles. Additionally, terms such as dehydrox (for dehydrogenation), 'FG' (flue gas), and 'FG LT' (flue gas, low temperature), which will be referenced in subsequent sections, are linked to these heat flows and the corresponding HEX

Figure 3 gives an overview of how the heat exchangers themselves operate. A heat source, based on the output of the energy converter, is matched with a heat requirement. In general, when available, the model uses the coolant to preheat the first part of the flow and then uses the spent fuel to preheat further. For the boron-based carriers, spent fuel and dehydrogenation heat from the reactor is not used for preheating. Not using this heat reduces complexity, prevents crystallisation in the spent fuel and removes a single point of failure. Flue gases are used to cover the final preheating and dehydrogenation heat. A minimum temperature difference between the heat source and heat sink of 10 K is assumed. If the heat sink and source differ, Figure 3 shows how this is handled. The equations in Figure 3 are all based on Equation (7). In the case of a larger heat sink, the final temperature of the fluid is calculated. When the heat source is larger, the mass of the heat source fluid can be adjusted to avoid huge heat exchangers. The model saves the heat content and maximum and minimum temperatures of a source or sink for detailed heat analyses. Whenever a source is insufficient to completely fill the need of a sink, an additional hydrogen burner will be used. This hydrogen burner reaches a temperature of 2480 K, the adiabatic flame temperature of hydrogen when combusted in air (Gupta and Pant 2008). The efficiency of the burner is calculated by using an efficiency of 95 % of the Carnot efficiency, with the cold sink being at the dehydrogenation temperature. The exact size of heat exchangers is not part of this research but has been done in another work of these authors (Van Rheenen et al. 2024).

3.3. Input parameters

The model requires several parameters to function. First of all, there is the energy requirement. In this paper, it is set to be 2 MJ. The rest of the parameters are divided into energy converter parameters

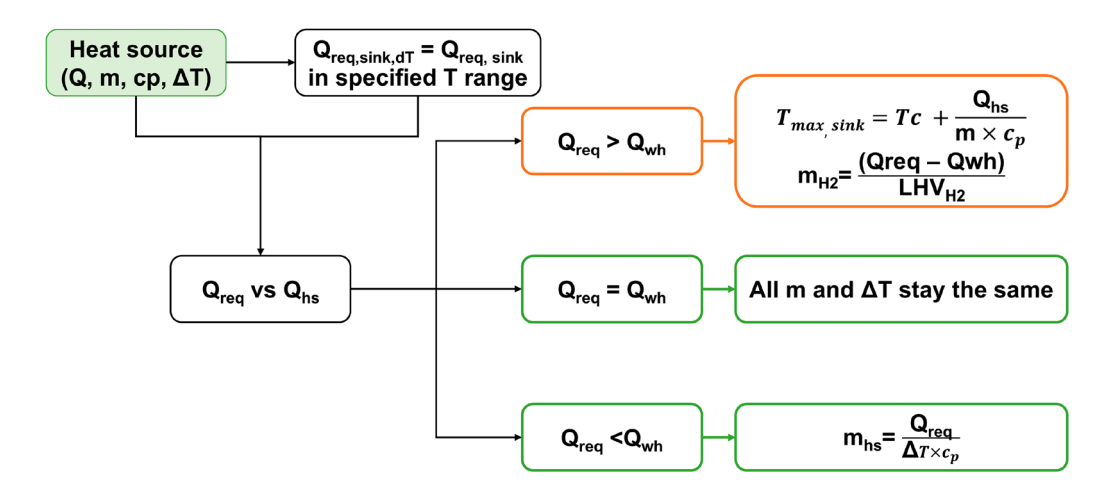


Figure 2. Heat flows and corresponding heat exchangers in the model.

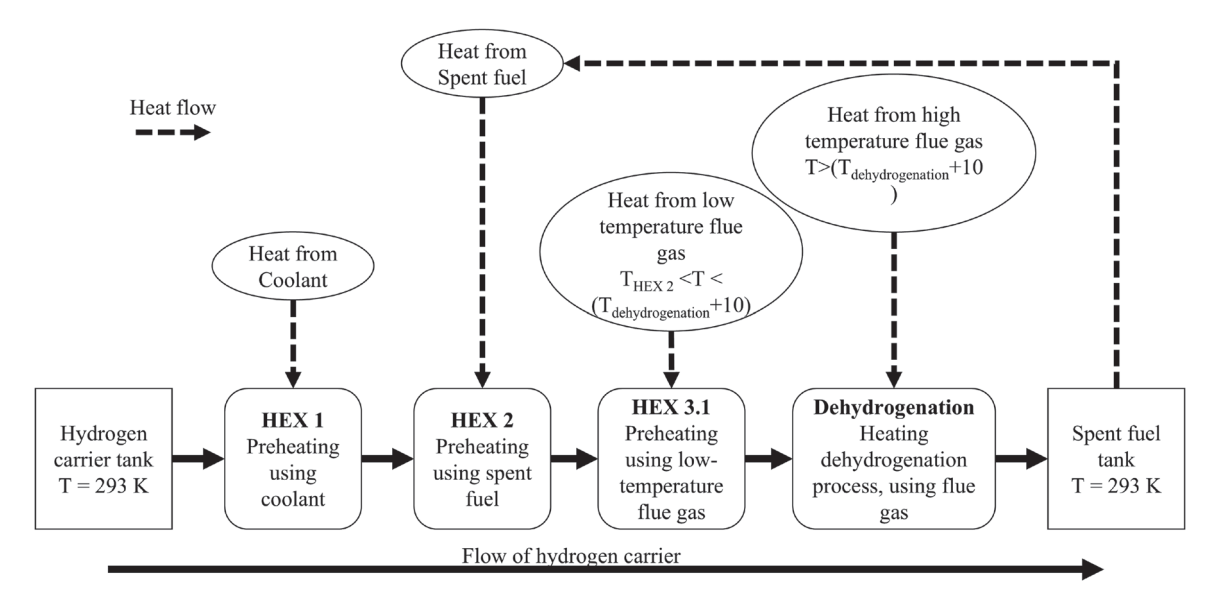


Figure 3. Representation of the heat exchangers inside the model.

Table 3. Parameters of hydrogen carriers, all parameters derived from (Lee et al. 2021; Kwak et al. 2021; Stark et al. 2015; Muller et al. 2015; Teichmann et al. 2012; Zhang et al. 2006; Kojima 2019; Ye et al. 2020; Damjanović et al. 2010; Chou and Chen 2015; Komova et al. 2016) and the Aspen database.

		•			
Parameter	DBT	NEC	SB	PB	AB
Hydrogen yield per molecule of hydrogen carrier [-]	9	6	4	4	3
Molecular weight [g/mol]	290.54	207	37.8	53.94	30.8
Heat capacity fuel [kJ/kgK]	1.96	2.04	4.54	3.48	4.54*
Heat capacity spent fuel [kJ/kgK]	1.82	1.56	N.R.	N.R.	N.R.
Dehydrogenation temperature [K]	573	503	353	353*	353*
Dehydrogenation energy [kJ/mol Fuel]	558	318	-210	-220	-156

Values denoted with * are estimated by the authors, as no precise information was available. N.R. stands for not relevant, this data is not required in the model

and hydrogen carrier parameters. Table 2 gives an overview of the parameters used in the energy converter section of the model, and Table 3 the parameters for the hydrogen carriers. This data is based on literature.

3.3.1. Energy converter parameters

The energy converter is approached as a component that divides the total amount of energy inside the hydrogen over several possible allocations:

$$E_{tot} = m_{H2} \cdot LHV_{H2} = E_{out} + Q_{coolant} + Q_{fg} + E_{loss}$$
 (8)

Here, E_{tot} is the total energy available in the mass. m_{H2} is the mass of hydrogen, and the LHV of hydrogen is 120 MJ/kg. E_{out} is the output energy, $Q_{coolant}$ the energy going to the coolant, Q_{fg} the energy going to the flue gases and E_{loss} the energy that cannot be recovered, all in MJ. This equation must always be true in the model; if it is false, it will run again. The model only uses the heat in the flue gasses at temperatures above the required threshold (for example, the dehydrogenation temperature). Equation (9) gives an overview of how this local heat source is derived from the total heat source.

$$Q_{local} = \frac{Q_{fg}}{\Delta T_{\text{max}}} \cdot \Delta T_{local} \tag{9}$$

The energy below this temperature cannot be used for heating and is thus excluded, adjusting the available (at the correct temperatures) flue gas energy accordingly.

The exact parameters defining the output values, as visible in Table 2, must always sum up to 100%. These parameters are all based on literature. However, due to a lack of available data, engines were chosen based on the amount of data available, not on the output power of the engine.

For example, the H2-ICE engine of Wang et al. (2019) has a maximum output power of 54.9 kW, while the user can choose the output energy of this model. Additionally, this engine runs in lean conditions to reduce NO_x emissions. The flue gas temperature strongly depends on whether the engine runs in lean or rich mixtures. However, lean operation is encouraged as the overall aim of using hydrogen carriers in this case is to reduce all emissions.

Unfortunately, sources looking at ammonia-hydrogen dual-fuel options usually consider only a small amount of hydrogen and can thus not be directly used. However, no alterations are considered in terms of overall efficiencies or outlet temperatures for the mixture of ammonia and hydrogen compared to hydrogen only. This assumption is based on the substantial quantity of hydrogen present in the feed (75% mole fraction, which contributes approximately 70% of the total energy) and the similarity of the efficiencies of hydrogen only and ammonia only (van Veldhuizen et al. 2023; Tornatore et al. 2022).

The ammonia generated from ammonia borane cannot be used directly in a PEMFC; it first has to be reformed to hydrogen. This reforming process incurs an energy penalty of 19 to 26 % (dependent on the cracking temperature) (Lee et al. 2021). While one mole of ammonia yields 1.5 moles of hydrogen, the initial reaction (seen in Equation (3)) produces 3 moles of hydrogen. The associated energy penalty, combined with increased system complexity, the need for additional control mechanisms, and extra equipment, renders the use of ammonia from ammonia borane impractical. However, certain catalysts enable the selective release of hydrogen directly from ammonia borane (Groom et al. 2019). Therefore, when utilising ammonia borane with a PEMFC, in this study only the hydrogen produced from the initial reaction is used, while the ammonia is not utilised.

For the PEMFC, relatively old data has been used (Zhao et al. 2017). More recent research shows that PEMFCs can reach efficiencies of up to 65% (Wang et al. 2022). However, efficiency is not the only parameter required in this research. Even though a PEMFC is actively cooled, there will always be energy lost to the environment that cannot be recovered. The losses in this model also include losses due to saturated oxygen lean air and traces of (purged) hydrogen. Additionally, energy is lost in the balance of plant and electrical transformers (Zhao et al. 2017). These power losses accumulate to a total of 12.3 %, but are likely to change with different efficiencies and types of PEMFCs. Thus, the data for PEMFCs in this research may be underestimated.

For the SOFC, data from van Veldhuizen et al. (2023) is used, even though Preuster et al. (2018) has already integrated a SOFC with a LOHC. As van Veldhuizen et al. (2023) reviews data from different papers and provides a detailed overview of mass and heat flows, the data from van Veldhuizen et al. (2023) is used in this study. The complementary information of van Veldhuizen et al. (2023) gives additional information needed to evaluate the parameters. The efficiency of the SOFC considers the fuel utilisation, and in this case, a fuel utilisation of 80% is considered. Most SOFCs in literature operate at this fuel utilisation (van Veldhuizen et al. 2023) as higher fuel utilisations may lead to unbalanced gas flows, resulting in corrosion and damage to the cells (Nishikawa et al. 2008). The remainder of the gas is combusted in an afterburner and the heat is used to preheat the fuel and air (van Veldhuizen et al. 2023). As the SOFC is air-cooled at high temperatures, the coolant power and temperatures are set to zero and the output cooling of the SOFC is treated as a flue gas.

The parameters of the gas turbine were based on data from Gohary and Seddiek (2013). However, the mass and energy balance in this model seemed incorrect. Consequently, we decided to adopt the provided efficiency value, assuming that it is accurate and consistent with similar systems. To make the energy balance feasible, we proposed reducing the mass flow of air going in the gas turbine, which would result in a thermodynamic balance. Additionally, we estimated thermal losses at approximately 9.5%, which aligns with typical values observed in ICEs and SOFCs, both of which operate as heat engines. This estimate is slightly lower but remains within a reasonable range, reflecting the expected heat losses for this type of system.

3.3.2. Hydrogen carrier parameters

Table 3 gives the specific parameters for the hydrogen carriers. Of these parameters, several are factual, such as the molecular weight and hydrogen yield per molecule, the latter of which is the maximum possible yield of pure hydrogen. The dehydrogenation temperatures are chosen to optimise reaction rates without compromising the hydrogen carrier. As for potassium borohydride and ammonia borane, no exact dehydrogenation temperatures are available. It is estimated that these reactions occur at the same temperature as sodium borohydride. The reaction processes are similar, even though the optimal temperature may differ depending on the catalyst. However, in this case, the same dehydrogenation temperatures were chosen. For the LOHCs, the heat capacity values of both the fuel and the spent fuel are calculated based on experimental values from Stark et al. (2015) and Muller et al. (2015). The heat capacity values are averages over 273 K to the dehydrogenation temperature. The heat capacity of the boron-based hydrogen carriers is more complicated. Boron-based hydrogen carriers are completely dissolved in water to avoid crystallisation (Andrieux et al. 2012). The heat capacity of the mixture is thus relevant. Due to the surplus water, the heat capacity of water is prevalent. The exact heat capacity of the mixture of 0.18 molar percentage sodium borohydride is calculated using the Aspen database. The same approach is used for potassium borohydride. The average values are shown in Table 3. For ammonia borane, the aspen database was insufficient. However, the molecular heat capacities for sodium borohydride and ammonia borane are very similar (86.8 J/molK at 298 K (Lide 2000) versus 81.4 J/molK at 323 K(Rassat et al. 2010). Additionally, the amount of water required to avoid crystallisation in the ammonia borane process is very similar, resulting in an estimated similar heat capacity of the fuel. The heat capacity of the spent fuel is not used to avoid crystallisation in the heat exchangers, which is likely to result in clogging.

4. Results

This section provides an overview of the model's results. The results include the additional water requirements (Subsection 4.1) and validation of results (Subsection 4.2). The energy distribution (Subsection 4.3) is also displayed. As a large amount of energy is lost through heat, Subsection 4.4 gives an overview of the detailed uses of heat. This way, possibilities for using waste heat can be found. The Sankey diagrams in Subsection 4.5 give a graphical representation of this heat uses, and additionally include the energy output. Finally, Subsection 4.6 showcases the effective energy density.

4.1. Additional water requirements

The hydrolysis dehydrogenation reaction requires water. Recycling this water from the outlet of the energy converter could completely satisfy the overall water requirements for all boron-based hydrogen carriers. However, as this recycling is most likely not 100%, we

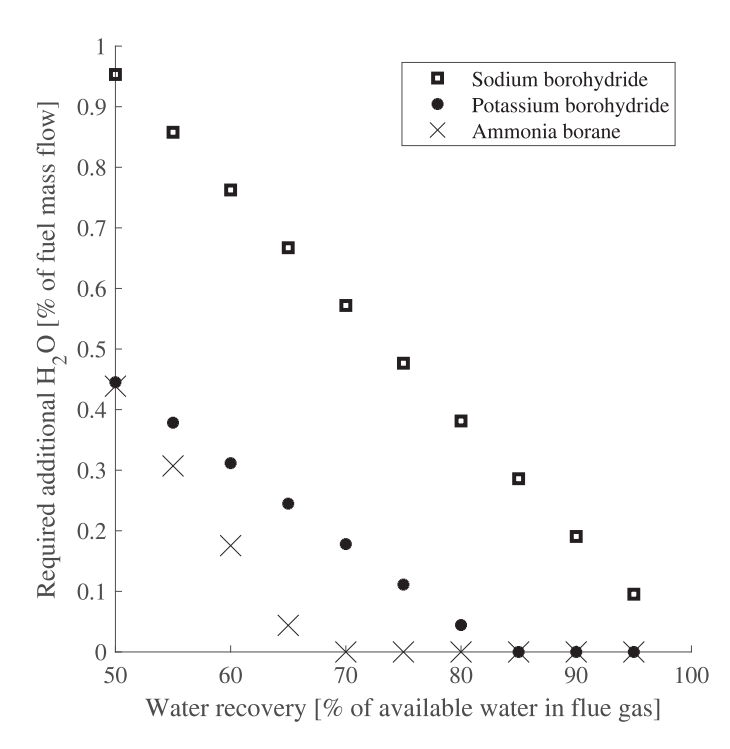


Figure 4. Effect of the water recirculation rate of water from exhaust gases on the amount of water that needs to be added to the system from an external source.

examined the water required for different recycling rates. Figure 4 shows the different recycling rates and resulting additional water requirements. An external pure water source is needed for sodium borohydride if the recycling rate is not 100%. Potassium borohydride will need an external water source when the recirculated water is less than 85%. However, in the case of ammonia borane, this external water source is only necessary for less than 70% of water recycling. Ammonia borane requires less water, and the conversion of ammonia and hydrogen also results in water.

4.2. Validation of results

We performed a pinch analysis on each total heat-exchanging system to verify whether the results were physically possible. A pinch diagram is a diagram in which each stream's temperatures and heat loads are plotted (Kemp and Shiun Lim 2020). To have a thermodynamically possible heat exchange, the hot stream must always be hotter than the cold stream. Crossing lines indicates a disagreement with the second law of thermodynamics. Additionally, a pinch diagram shows where the design is most constrained, namely where the hot and cold lines are closest. This point is called a pinch.

Pinch analyses were used for each of the configurations possible in the model. Figure 5 gives an example of a pinch analysis, in this case, of dibenzyltoluene and an internal combustion engine. The pinch analysis provides additional information, such as that the heat from the flue gases is insufficient in covering the dehydrogenation heat; additional heat from hydrogen burning is required.

4.3. Energy distribution

The energy distribution analysis, represented in Figures 6–10, shows the energy distribution throughout the system, organised per hydrogen carrier. These figures show the delivered energy, energy in the coolant and the flue gases, additional energy added through a burner and absolute or irrecoverable losses. All combinations deliver the

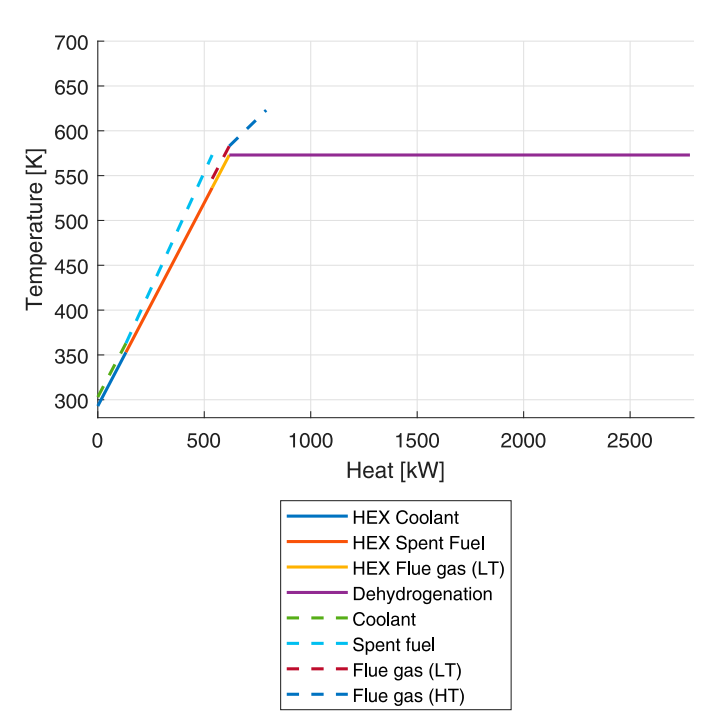


Figure 5. Pinch analysis of dibenzyltoluene combined with an internal combustion engine.

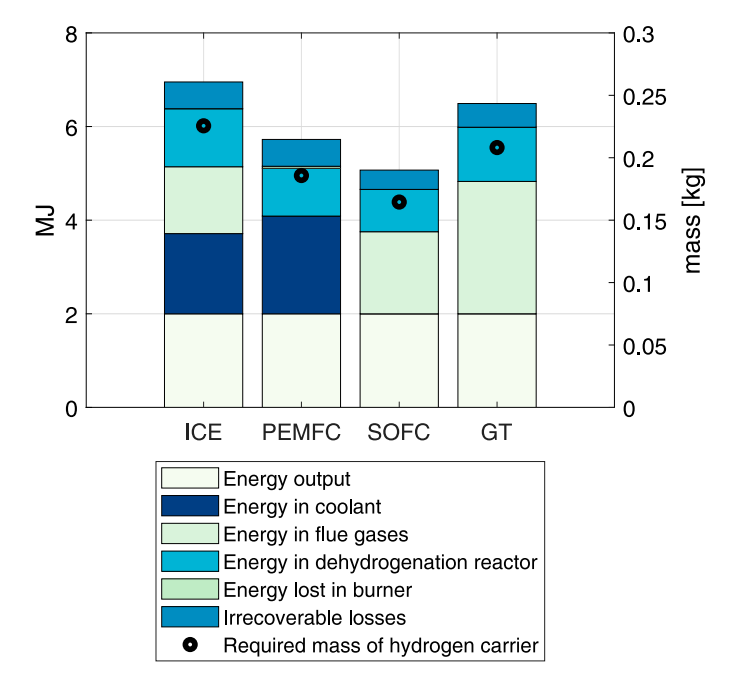


Figure 6. Energy distribution of sodium borohydride.

same output energy, in this case, 2 MJ. The mass of energy is also plotted in the figures.

Figures 6 and 7 show the energy distribution of the borohydrides. Potassium borohydride (Figure 7) has a very similar energy contribution as sodium borohydride (Figure 6), but does have an overall higher mass. Figure 6 shows the influence of the efficiency of the energy converter; a higher efficiency results in a lower mass of sodium borohydride.

Figure 8 shows the energy distribution of ammonia borane. The heat produced in the reactor is much less for ammonia borane than the borohydrides' heat production. Additionally, this heat is less than

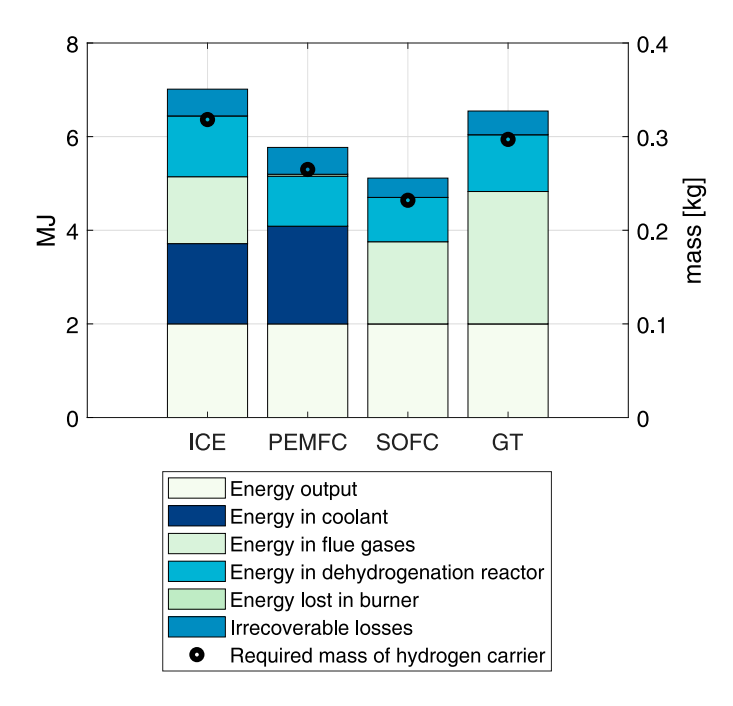


Figure 7. Energy distribution of potassium borohydride.

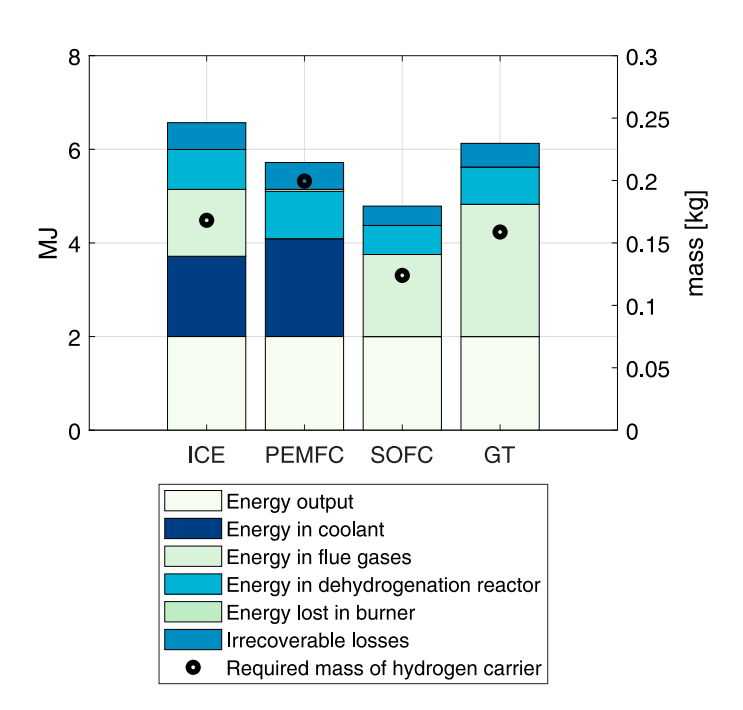


Figure 8. Energy distribution of ammonia borane.

the heat in the coolant and the flue gases. The combination of NH_3 and H_2 produces more power in an absolute sense, thus reducing the required mass. This is also clear when removing the NH_3 , as done for the PEMFC. With only hydrogen, the mass required to deliver the same energy is much higher.

Figures 9 and 10 show the energy distribution of the LOHCs. Figure 9 shows that a hydrogen burner is always necessary for DBT, even though it only has to provide approximately 15 kW in the SOFC-coupled scenario. Figure 10 shows that both the SOFC and the GT give enough heat for NEC's preheating and dehydrogenation process, as the overall heating requirements are lower for NEC than for DBT.

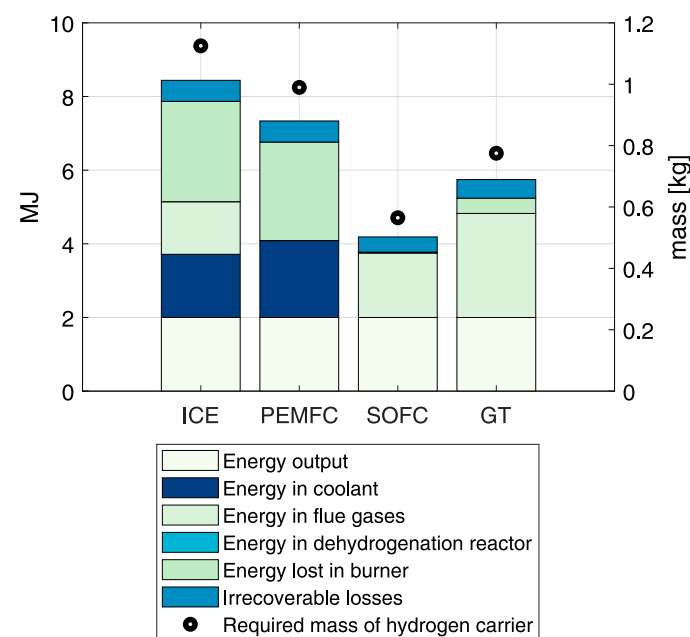


Figure 9. Energy distribution of dibenzyltoluene.

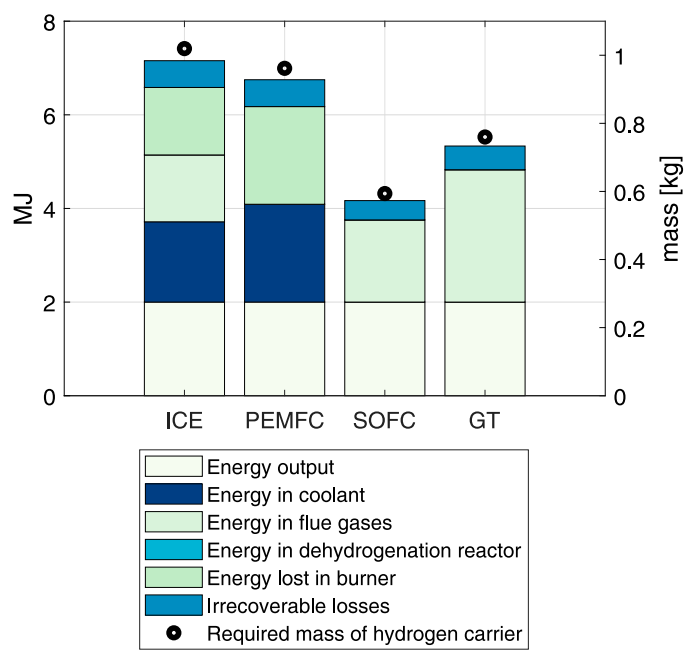


Figure 10. Energy distribution of n-ethylcarbazole.

4.4. Detailed use of heat

Theenergy converters produce large amounts of heat, as only between 35 and 48% of hydrogen's total energy is converted to effective work. The rest of the energy becomes heat. Part of this heat is used for preheating fuel and dehydrogenation when necessary. In other cases, the dehydrogenation process produces more heat. A detailed analysis of the heat sinks and sources of the energy converter and the reactor offers insight into the quality of heat and the amount of heat left over. This gives insight into whether the heat can be used for other processes onboard. The detailed distributions of heat are visible in Figures 11–15.

Boron-based carriers produce heat during the dehydrogenation process. Figures 11–13 show these amounts of heat. Ammonia

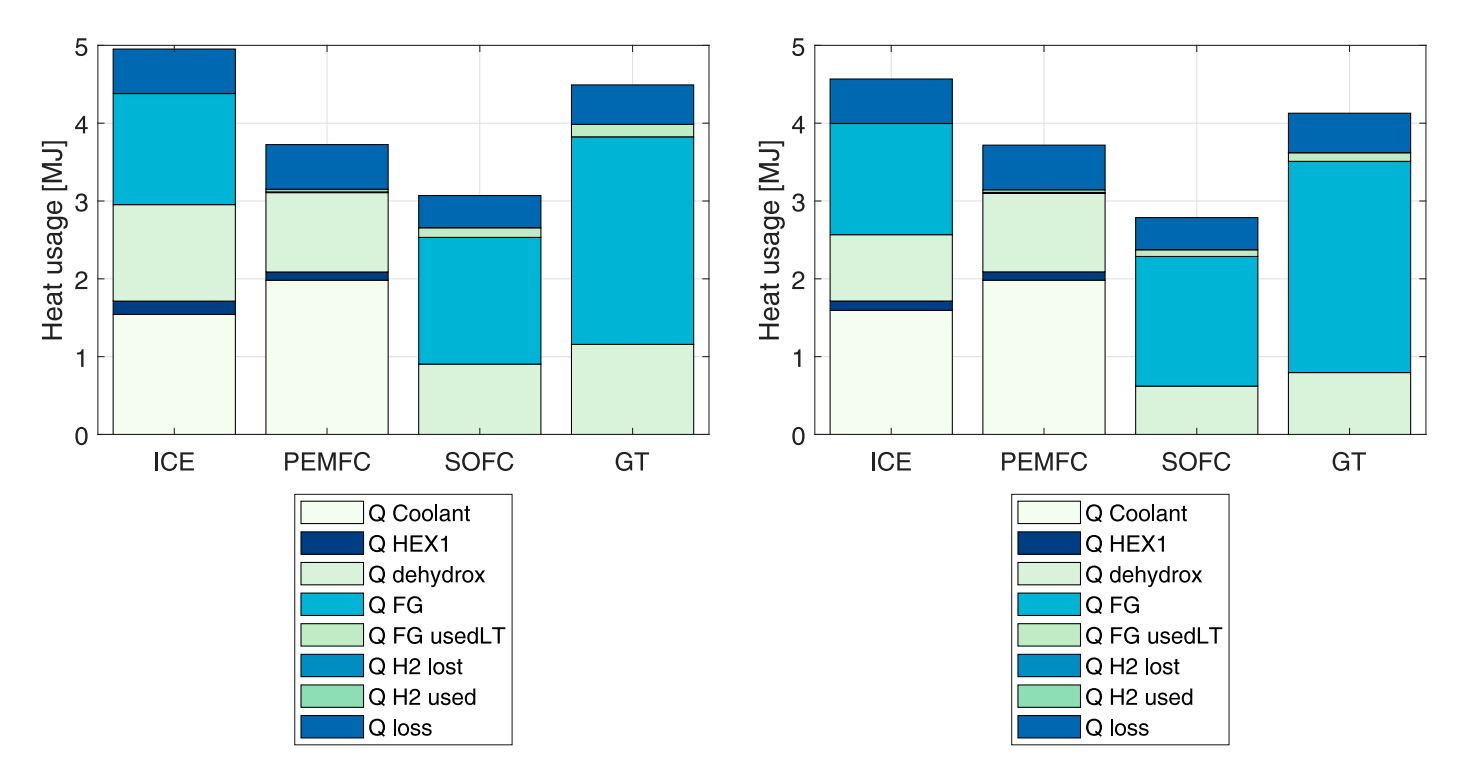


Figure 11. Distribution of heat for sodium borohydride.

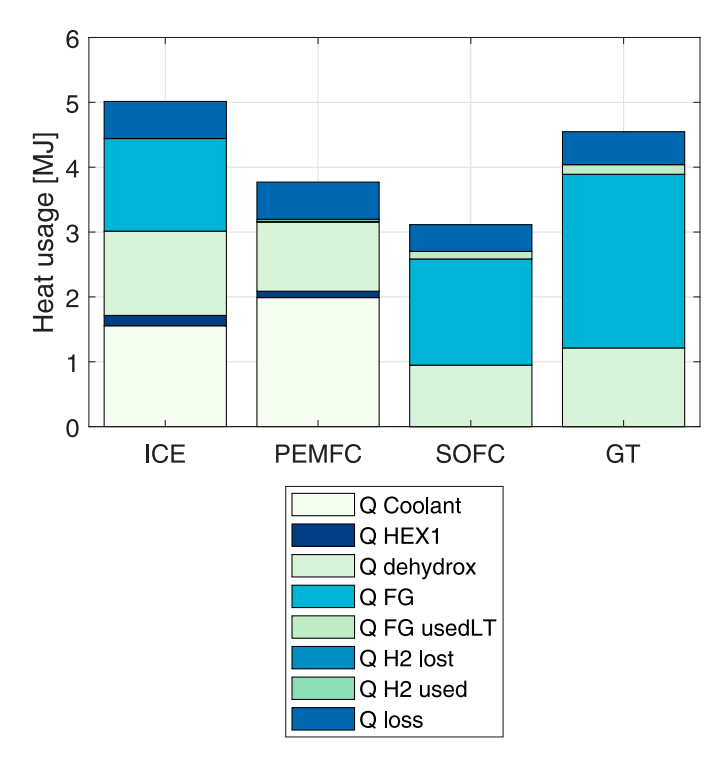


Figure 12. Distribution of heat for potassium borohydride.

borane produces less heat during dehydrogenation compared to the borohydrides, resulting in lower cooling requirements. A small amount of heat is required for preheating. Coolants and flue gases are used for preheating. Only for the combination of a PEMFC is a hydrogen burner required, as the average output temperatures of a PEMFC are too low to reach the desired temperature of the fuel.

Figures 14 and 15 show the heat distribution of DBT and NEC, respectively. Despite the large amount of available heat, hydrogen

Figure 13. Distribution of heat for ammonia borane.

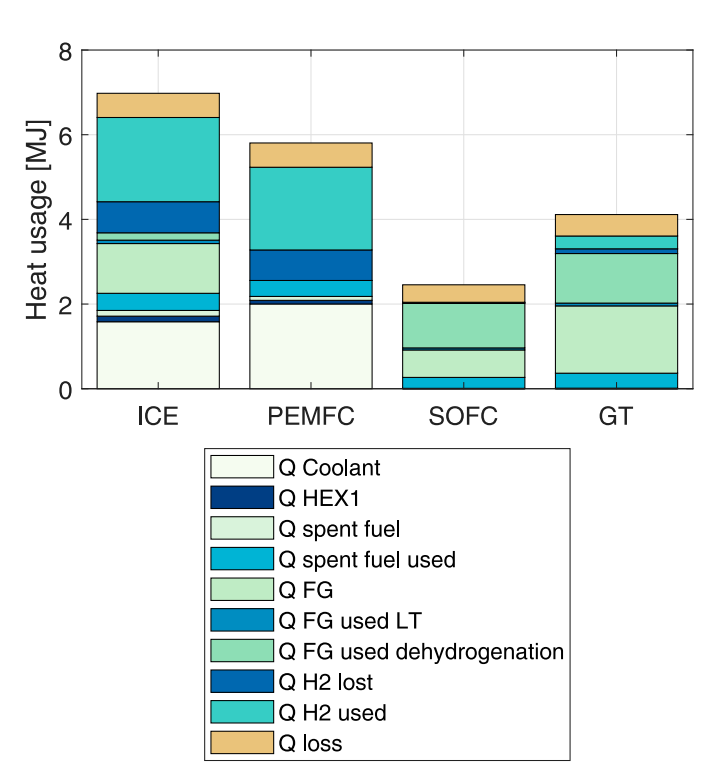


Figure 14. Distribution of heat for dibenzyltoluene.

burning is always required for DBT, as much of the heat is too low quality. High-temperature flue gas heat is the only heat available for dehydrogenation. Most of this high-quality heat is available in the SOFC and GT flue gases. As NEC has lower dehydrogenation requirements, its heat requirement can be covered when integrating with a SOFC and GT.

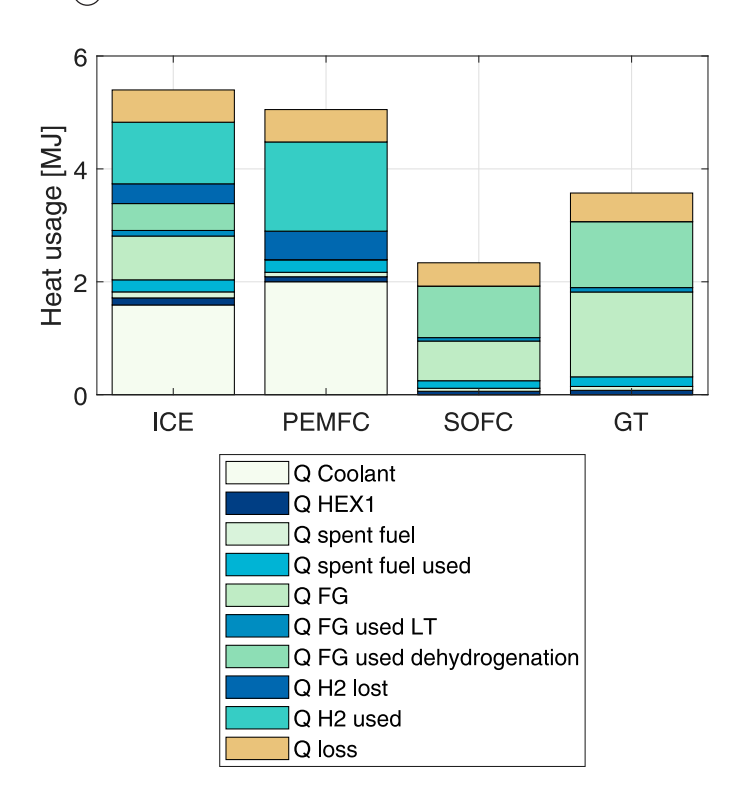


Figure 15. Distribution of heat for n-ethylcarbazole.

4.5. Overview of all energy flows

Sankey diagrams can be used to get a graphical overview. A Sankey diagram provides an overview of all energy flows within a process. We made Sankey diagrams for four combinations of energy converters and hydrogen carriers. These Sankey diagrams graphically represent cases with the same underlying data as provided in the previous subsection (Subsection 4.4). Thee Sankey diagrams are meant to give an overview of the relevant processes in the integration of hydrogen carriers. To get correct Sankey diagrams, the enthalpy of all fluids has to be used. However, as these diagrams are meant to illustrate the process and its relevant energy flows, the lower heating value of hydrogen is used to calculate the energy flows.

We cover the combinations of DBT and a GT, which will require limited hydrogen heating and NEC and a SOFC, which requires no hydrogen heating. As ammonia borane in combination with a PEMFC is an oddity, a Sankey diagram of ammonia borane with an ICE is made and the PEMFC and sodium borohydride are visualised in another diagram. Potassium borohydride is not covered in the Sankey diagrams, as it is thermodynamically very similar to sodium borohydride but has a lower energy density.

Figure 16 shows a Sankey diagram for ammonia borane coupled with an ICE. The waste heat of the reactor and the coolant form a large, low-quality heat sink, while the flue gasses form a significantly high-quality heat sink.

Figure 17 shows sodium borohydride coupled to a PEMFC. The heat provided by the PEMFC is of too low temperature to preheat the fluid fully. However, Figure 17 clearly shows that the resulting hydrogen heating flow is minimal and is thus not a large energy loss.

Figures 18 and 19 give an overview of typical Sankey diagrams for LOHCs. Both Sankey diagrams show large heat flows returning to the reactor to provide sufficient heat for the dehydrogenation process. Figure 18 shows a small hydrogen flow required for preheating. This flow becomes larger when there are smaller high-temperature heat sinks. Figure 18 clearly shows that, in this case, the required hydrogen

for dehydrogenation is minimal and only slightly influences the overall energy density. Figure 19 shows no additional heating is required for NEC coupled with a SOFC. The overall input energy is much less than the overall input energy of DBT combined with a gas turbine, indicating a much higher efficiency.

4.6. Effective energy density

Figure 20 shows the effective energy density of each fuel, as well as the effective energy density of marine diesel oil (MDO). Data for MDO is taken from (Gohary and Seddiek 2013; van Veldhuizen et al. 2023), while data for compressed hydrogen comes from (Rivard et al. 2019). The data from Rivard et al. (2019) reflect the ultimate goal of the United States Department of Energy for the gravimetric energy density of compressed hydrogen. In this case, the effective energy density is the amount of mechanical or electrical energy that can be taken from 1 kg of fuel. This definition includes the energy converter, as heat and mass integration is necessary to use hydrogen carriers efficiently.

Table 4 gives an overview of the relevant masses of the hydrogen carrier and the pure hydrogen they carry. As sodium borohydride and potassium borohydride do not require hydrogen heating, their hydrogen mass is the same. This also applies to ammonia borane in combination with a PEMFC, as then only hydrogen is required. For the other energy converters, ammonia borane has less hydrogen content, as part of the energy is covered by ammonia. The table also clearly shows that both LOHCs not only have larger masses themselves, but the amount of hydrogen they require is often also more. As hydrogen is often required for preheating and dehydrogenation, more hydrogen is required to reach the same energy in total.

This hydrogen demand is governed by the maximum efficiency of the hydrogen burner, which in this study is modelled at 95% of the Carnot efficiency. This adjustment accounts for losses due to imperfect isolation, possible incomplete combustion and other practical inefficiencies. While the use of Carnot efficiency for a furnace is justified, De Saro (2008) suggests incorporating ambient temperature into the calculation for a more accurate assessment. In our current model, accounting for this different efficiency results in minimal output changes. For dibenzyltoluene, the mass of the hydrogen carrier is affected in all four cases: internal combustion engine $(-0.06 \,\mathrm{kg})$, PEMFC (-0.07 kg), SOFC (-0.01 kg) and GT (-0.01 kg). For nethylcarbazole, only the internal combustion engine (-0.02 kg) and PEMFC (-0.04 kg) were affected. Although these differences are relatively small, they demonstrate the flexibility of the model. The ability to accommodate variations in input parameters while producing consistent results underscores the robustness of the approach.

5. Discussion

For hydrogen carriers to be relevant as future fuels, their energy density has to be identified. This discussion section will discuss the overall energy density and additional requirements for each of the hydrogen carriers.

5.1. Sodium borohydride, potassium borohydride and ammonia borane

Sodium borohydride and potassium borohydride are very similar substances, while ammonia borane has similar chemical properties as both of them. A great advantage of potassium borohydride as compared to sodium borohydride would be the reduction of additional water, if not all water can be recycled. A recycling rate of 100%, however, is likely to be only practical when using a PEMFC (Yamada and Mohamad 2010). Removing water from flue gases by cooling the flue

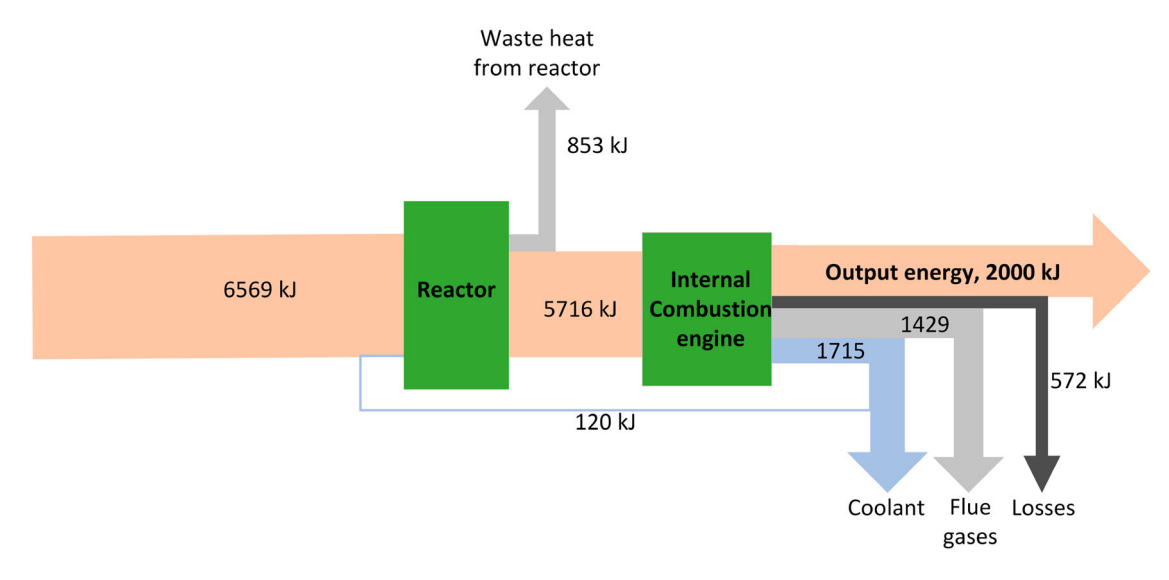


Figure 16. Sankey diagram of ammonia borane coupled with an internal combustion engine.

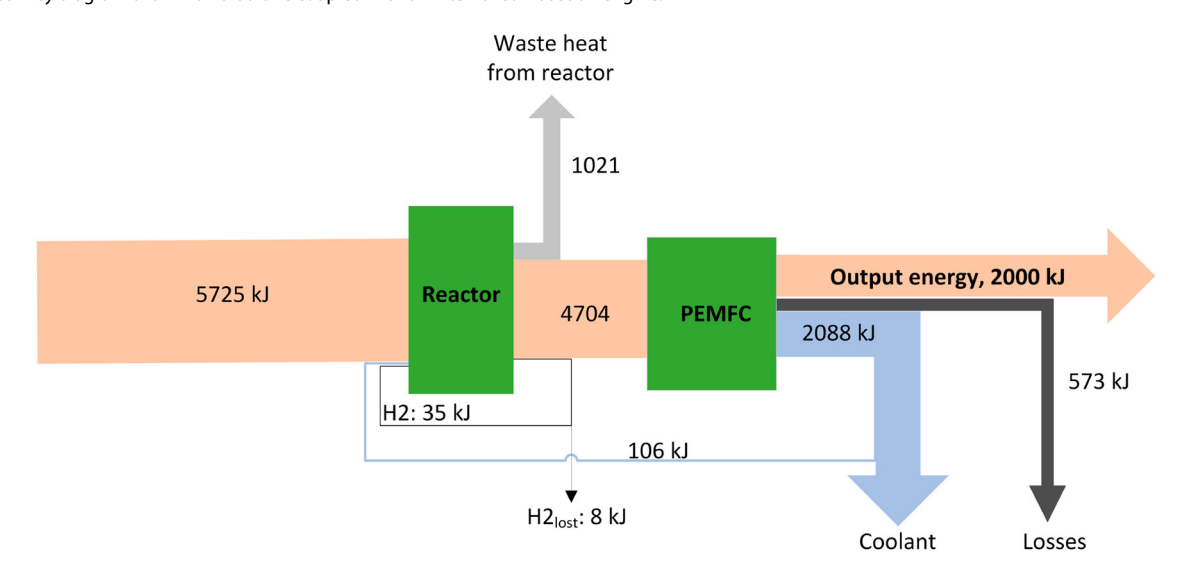


Figure 17. Sankey diagram of sodium borohydride coupled with a PEMFC.

gas to a water condensation temperature may influence the operating conditions and thus the efficiency of an internal combustion engine or a gas turbine, resulting in a limit of approximately 50% of water recycling. Anode off-gas recirculation, including water recycling and condensation, is often used in SOFCs (Peters et al. 2016). The anode off-gas recirculation rate influences the efficiency of the system, extracting 100 % of the produced water will likely result in a lower efficiency (Peters et al. 2016). Thus, potassium borohydride with a PEMFC has advantages if a closed loop is desired. Closed loops are less relevant onboard ships, where unlimited water is available.

The energy density of the boron-based carriers is influenced by their exothermic nature. Part of the overall energy available is lost to heat during dehydrogenation. As this is percentage-wise larger for potassium borohydride than for sodium borohydride, potassium borohydride requires a significantly larger mass to reach the same energy output. It is the least for ammonia borane, which results in it requiring the lowest mass and, thus, reaching the highest energy density.

Although ammonia is produced by ammonia borane, pure ammonia is still excluded from this study, necessitating further explanation. First, the safety requirements for ammonia borane differ significantly from those for pure ammonia. While ammonia borane

does release ammonia, it does so in much smaller quantities, and this ammonia is likely to be consumed immediately by the engine. If needed, a buffer could consist of pure hydrogen instead. Additionally, the amount of ammonia produced is lower than the hydrogen output and several liters of ammonia compared to storing the entire energy source as ammonia results in a critical safety distinction that we believe cannot be overlooked. Secondly, when considering ammonia as a hydrogen carrier, the cracking temperature required is notably higher than that of other carriers, such as DBT, which already poses challenges for integration with available heat sources, as we have demonstrated previously.

Generally, due to the exothermic nature of the hydrolysis process, a lot of high- and low-quality heat is available for other onboard systems. Low-quality heat is more challenging to use than high-quality heat.

5.2. LOHCs

DBT and NEC have similar energy densities, but there are still several differences. The mass of hydrogen carrier required to reach the energy output is lower for DBT, except when coupled to an internal combustion engine. Additional heating when combining DBT



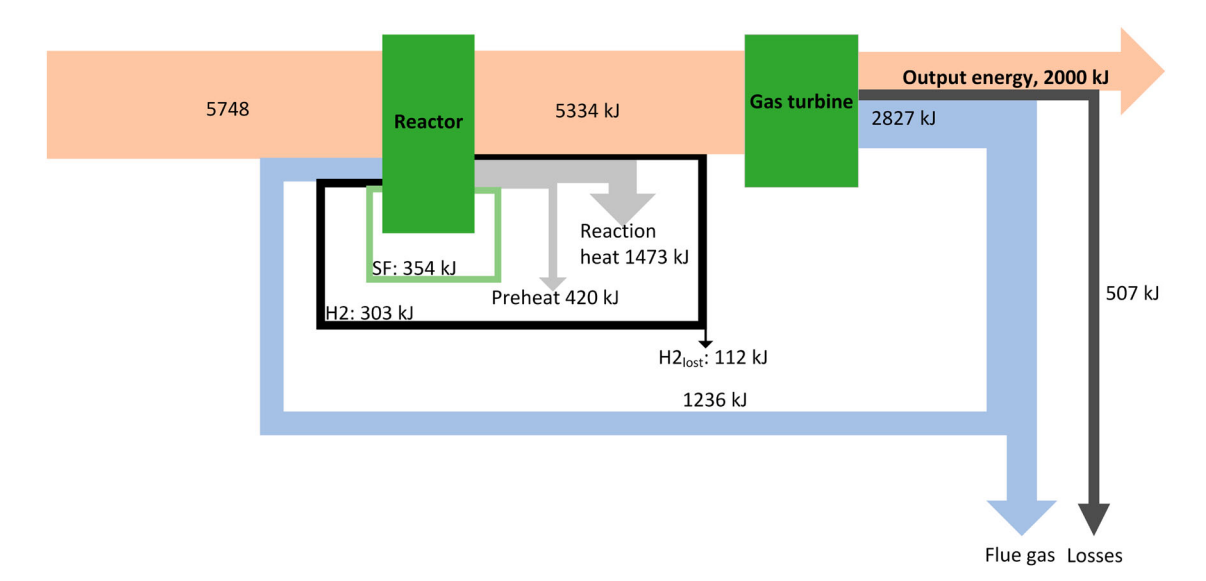


Figure 18. Sankey diagram of DBT coupled with a gas turbine.

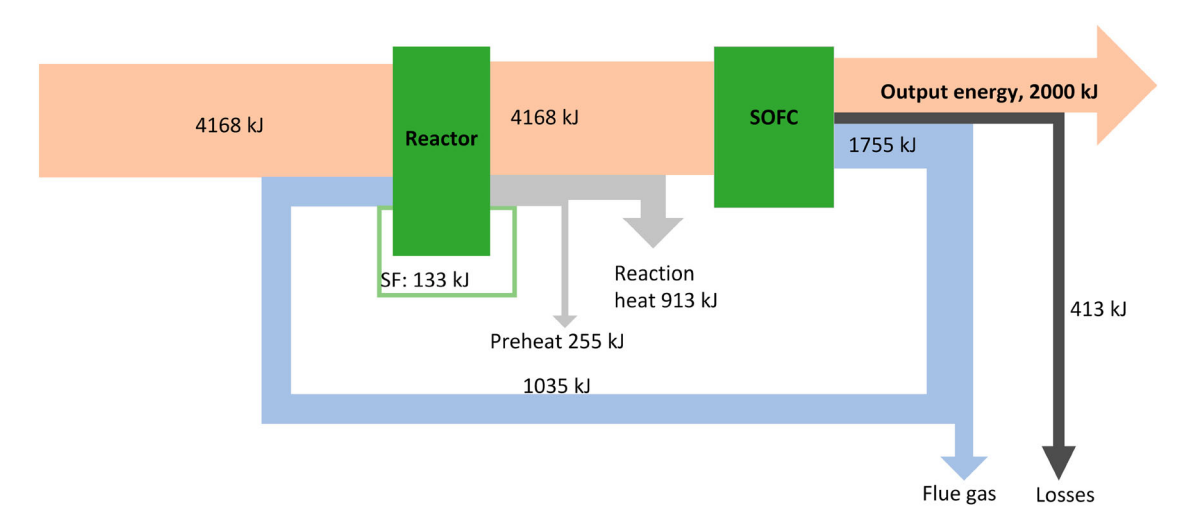


Figure 19. Sankey diagram of NEC coupled with a SOFC.

with an internal combustion engine causes this higher mass. However, especially for the ICE, a large percentage of the heat in the flue gas is at temperatures too low for dehydration. This is even stronger for DBT (see Figure 14) than for NEC due to DBTs higher dehydrogenation temperature. As DBT has a higher hydrogen content, the overall mass is smaller with excellent heat integration. The SOFC scenarios endorse this, as very little additional heating is required when using DBT. The integration of dehydrogenation is more effective for NEC than for DBT. This suggests that the choice of LOHC may not be as important as the efficiency of the energy converter. However, as the LOHCs have such similar energy densities, other factors such as technology readiness levels, safety or handling, are likely to be the decisive factor in choice between LOHCs.

5.3. Comparison and overall energy density

The effective energy densities of ammonia borane and sodium borohydride are the highest, irrespective of the used energy converter. Potassium borohydride has a much lower energy density than sodium borohydride on all accounts. Additionally, the highest energy efficiency for potassium borohydride (when combined with an SOFC) still does not come close to the lowest effective energy density of sodium borohydride (when combined with an ICE). Thus, potassium borohydride is generally less energy dense.

Despite their different theoretical energy densities, Figure 20 shows very little difference between the LOHCs. Both LOHCs have energy densities much lower than the other hydrogen carriers or MDO. Up to five times more LOHC is required to have a similar energy density as MDO. However, the LOHCs may be able to reach very similar energy densities as compressed hydrogen (which is here estimated to have a gravimetric energy density of 6.5 wt% of hydrogen, the ultimate DOE goal (Rivard et al. 2019)). A large difference in effective energy density exists between the boron-based carriers and the LOHCs. There are two main reasons for this. Firstly, the endothermic nature of the LOHCs results in higher masses of the hydrogen carrier than the boron-based carriers. Secondly, the LOHCs store less hydrogen per kilogram, theoretically, than boronbased carriers.

The effective energy density is strongly influenced by the energy converter. An energy converter with a higher efficiency will result in a higher effective energy density. The energy density of ammonia borane when using a gas turbine differs only slightly from MDO combined with a gas turbine. The energy density of sodium borohydride is lower than that of MDO for each of the combinations but does appear to be in a similar ballpark. On the other hand, the energy

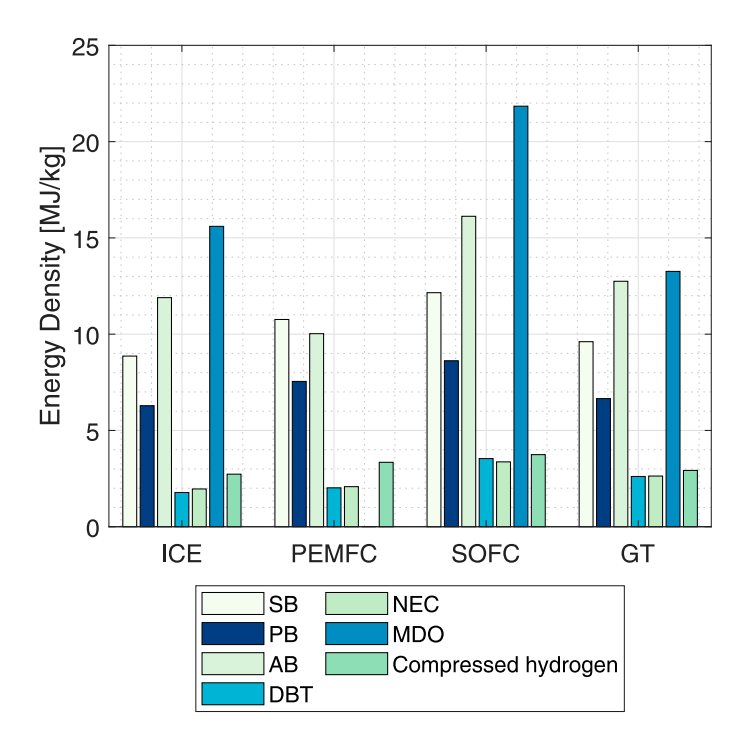


Figure 20. Effective energy density of the discussed hydrogen carriers, excluding the influence of the spent fuel.

Table 4. Mass of hydrogen into the engine and mass of hydrogen carrier, to have an 2 MJ energy output.*For ammonia borane, only the hydrogen mass is shown in this table, the ammonia is not shown here, but does influence the overall energy density.

	SB	PB	AB*	DBT	NEC	
ICE	0.048	0.048	0.033	0.070	0.060	Hydrogen to engine
ICE	0.225	0.318	0.168	1.125	1.020	Hydrogen carrier
PEMFC	0.039	0.039	0.039	0.061	0.056	Hydrogen to engine
PEMFC	0.186	0.264	0.200	0.990	0.962	Hydrogen carrier
SOFC	0.035	0.035	0.024	0.035	0.035	Hydrogen to engine
SOFC	0.165	0.232	0.124	0.565	0.594	Hydrogen carrier
GT	0.044	0.044	0.031	0.048	0.044	Hydrogen to engine
GT	0.211	0.300	0.157	0.766	0.760	Hydrogen carrier

density of ammonia borane with an SOFC surpasses the combination of MDO with a GT and with an ICE. Thus, ammonia borane and sodium borohydride have high energy densities, on par with or at least similar to current technologies.

6. Conclusion

This study aimed to evaluate the effective energy density of hydrogen carriers as alternative fuels. We accomplished this goal by examining the efficiency of the overall energy cycle when using alternative fuels. Our model can calculate different efficiencies in a simple, yet accurate manner, enabling us to conclude the efficiency and, thus, the practicability of hydrogen carriers.

Themodel consists of two main types: the dehydrogenation process can be either end or exothermal. However, this dehydrogenation process always requires either energy (in the form of heat) or mass (e.g. water). To determine the overall energy density of the system, we built a thermodynamic 0D model which integrates the heat and masses of the system. This model provided a first indication of the overall energy densities of five hydrogen carriers combined with four energy converters, which are as follows.

Sodium borohydride and ammonia borane have the highest energy densities of the hydrogen carriers. Without taking the spent fuel into account, these energy densities are close to (and may, in some cases, even surpass) the energy density of diesel. Although both LOHCs have lower energy densities, similar to that of compressed hydrogen, other characteristics may still make them relevant. Potassium borohydride, on the other hand, is not as favourable as sodium borohydride.

Our study highlights the importance of heat and mass integration of hydrogen carriers and energy converters for the overall energy density. Although the 0D model only provides estimates, it shows compelling findings, which should be investigated in more detail in future research. Hydrogen carriers can achieve overall energy efficiencies similar to conventional fuels, thereby considerably enhancing the attractiveness of more sustainable options.

7. Future research

The current model provides a simplified but well-founded overview of the effective energy efficiency and density of the different combinations of hydrogen carriers and energy converters. This overview could be improved with more specific temperature and heat distributions of the energy converters and by looking at load factors. These parameters largely depend on the operating conditions and the power requirements of ships, making them different for different ship types and operational profiles.

The input values of the model are based on data from the literature. However, especially for the efficiencies of the energy converters, controversies exist. For example, hydrogen-powered SOFCs have efficiencies ranging from 37.5 to 49.6% (van Veldhuizen et al. 2023). A sensitivity analysis can be used to determine whether the heat requirements can still be fulfilled when other efficiencies are used. This is especially relevant for the converters producing higher-quality heat (ICE, GT and SOFC) combined with the LOHCs.

The model currently calculates the gravimetric energy density. As some ships are volume-limited, the volumetric energy density is also interesting. Calculating this volumetric energy density can be easily done for the LOHCs. LOHCs are generally fluids in the hydrogenated and dehydrogenated states, and their density is clearly defined. The boron-based carriers, however, are powders. Powders have a bulk and particle density (Mukhopadhyay et al. 2019). The differences between these densities can be large and are influenced by the moisture content and particle size (Mukhopadhyay et al. 2019).

In addition to the energy density, power density is important for all ships. To provide a more complete overview, the power density of each of the options should be evaluated. However, the technology readiness levels of the hydrogen carriers are not yet sufficient for this power density analysis. Besides power density, other properties of hydrogen carriers influence the possible use of fuel, such as safety, handling, availability and costs, which is closely related to the recycling process of the spent fuel.

The model can be enhanced for more detailed results. In the exothermic model, cooling of waste heat is currently not considered, even though cooling pumps will cost power. Using this waste heat for other purposes, such as co-generation or hotel loads, can enhance the system's energy efficiency, particularly for boron-based carriers. Additionally, the cracking of ammonia could be considered. It would also add the PEMFC as an option for ammonia borane. The endothermic model could be enhanced by optimising the heat integration to avoid too high heat loads on the reactor, as done in (Preuster et al. 2018). However, all combined, the model provides a good first overview of the possibilities that hydrogen carriers and energy converters can provide.



Acknowledgments

This work is an extension of a conference paper presented at MOSES 2023 (Van Rheenen, E.S., Padding, J.T., Visser., 2023. A 0D Model for the Comparative Analysis of Hydrogen Carriers in Ship's Integrated Energy Systems. Conference Proceedings of MOSES, doi:10.59490/moses.2023.669)

Disclosure statement

No potential conflict of interest was reported by the author(s).

Funding

This work was supported by the project SH2IPDRIVE: Sustainable Hydrogen Integrated Propulsion Drives, funded by the Rijksdienst voor Ondernemend Nederland (RVO) under grant MOB21013

ORCID

Erin S. van Rheenen http://orcid.org/0009-0001-4607-5281

References

- Andrieux J, Laversenne L, Krol O, Chiriac R, Bouajila Z, Tenu R, Counioux JJ, Goutaudier C. 2012. Revision of the NaBo₂–H₂O phase diagram for optimized yield in the H2 generation through NaBh₄ hydrolysis. Int J Hydrogen Energy. 37(7):5798–5810. doi: 10.1016/j.ijhydene.2011.12.106 XII International Symposium on Polymer Electrolytes: New Materials for Application in Proton Exchange Membrane Fuel Cells.
- Aronietis R, Sys C, van Hassel E, Vanelslander T. 2016. Forecasting port-level demand for lng as a ship fuel: the case of the port of antwerp. J Ship Trade. 1(2). doi: 10.1186/s41072-016-0007-1
- Bonnetot B, Laversenne L. 2005. Hydrogen storage using borohydrides. Ann Chim Sci Mater. 30:495–503.
- Chou CC, Chen BH. 2015. Hydrogen generation from deliquescence of ammonia borane using ni–co/r-go catalyst. J Power Sources. 293:343–350. doi: 10.1016/j.jpowsour.2015.05.091
- Damjanović I, Bennici S, Auroux A. 2010. A direct measurement of the heat evolved during the sodium and potassium borohydride catalytic hydrolysis. J Power Sources. 195(10):3284–3292. doi: 10.1016/j.jpowsour.2009.11.105
- De Saro R. 2008. Thermal efficiency limits for furnaces and other combustion systems. J Thermophys Heat Transf. 22(3):532–537. doi: 10.2514/1.28239
- Dimitriou P, Tsujimura T. 2017. A review of hydrogen as a compression ignition engine fuel. Int J Hydrogen Energy. 42(38):24470–24486. doi: 10.1016/j.ijhydene.2017.07.232
- Düll A, Rohlfs P, Deutschmann O, Börnhorst M. 2022. Performance evaluation of KBH₄ as energy carrier for shipping applications. Chem Ing Tech. 94(5):747–759. doi: 10.1002/cite.v94.5
- Fatsis A. 2022. Gas turbine performance enhancement for naval ship propulsion using wave rotors. J Mar Eng Technol. 21(5):297–309. doi: 10.1080/20464177. 2021.1933697
- Gohary MME, Seddiek IS. 2013. Utilization of alternative marine fuels for gas turbine power plant onboard ships. Int J Nav Archit Ocean Eng. 5(1):21–32. doi: 10.2478/IJNAOE-2013-0115
- Groom TB, Gabl JR, Pourpoint TL. 2019. Portable power generation for remote areas using hydrogen generated via maleic acid-promoted hydrolysis of ammonia borane. Molecules. 24(22):4045. doi: 10.3390/molecules24224045
- Gupta R, Pant K. 2008. Fundamentals and use of hydrogen as a fuel. CRC Press. p. 2–32.
- IMO. 2023. Revised ghg reduction strategy for global shipping adopted; [https://www.imo.org/en/MediaCentre/PressBriefings/pages/Revised-GHG-reduction-strategy-for-global-shipping-adopted-.aspx].
- International Energy Agency. 2021. International shipping. Paris. Accessed on 22nd June 2022; https://www.iea.org/reports/international-shipping.
- Kass MD, Sluder CS, Kaul BC. 2021. Spill behavior, detection, and mitigation for emerging nontraditional marine fuels. Oak Ridge National Laboratory. Report No:.
- Kemp IC, Shiun Lim J. 2020. Chapter 3 key concepts of pinch analysis. In: Kemp IC, Shiun Lim J, editors. Pinch analysis for energy and carbon footprint reduction (third edition). 3rd ed. Oxford, UK: Butterworth-Heinemann, p. 35–61.
- Kojima Y. 2019. Hydrogen storage materials for hydrogen and energy carriers. Int J Hydrogen Energy. 44(33):18179–18192. doi: 10.1016/j.ijhydene.2019.05.119
- Komova O, Kayl N, Odegova G, Netskina O, Simagina V. 2016. Destabilization of nh3bh3 by water during hydrothermolysis as a key factor in the high hydrogen evolution rates. Int J Hydrogen Energy. 41(39):17484–17495. doi: 10.1016/j.ijhydene.2016.07.163

- Krol O, Andrieux J, Counioux JJ, Tenu R, Goutaudier C. 2009. Solubility and related equilibria in the KBO2 – H2O and KBO2 – H2O – KOH systems. JEEP – Journées D'Etude Des Equilibres Entre Phases. 00023.
- Kwak Y, Kirk J, Moon S, Ohm T, Lee YJ, Jang M, Park LH, Jeong H, Sohn H. 2021. Hydrogen production from homocyclic liquid organic hydrogen carriers (LOHCs): benchmarking studies and energy-economic analyses. Energy Convers Manag. 239:114124. doi: 10.1016/j.enconman.2021.114124
- Lee S, Kim T, Han G, Kang S, Yoo YS, Jeon SY, Bae J. 2021. Comparative energetic studies on liquid organic hydrogen carrier: a net energy analysis. Renew Sustain Energy Rev. 150:111447. doi: 10.1016/j.rser.2021.111447
- Li L, Aravind PV, Woudstra T. 2023. Assessing the waste heat recovery potential of liquid organic hydrogen carrier chains. Energy Convers Manag. 276:116555. doi: 10.1016/j.enconman.2022.116555
- Lide DR. 2000. CRC handbook of chemistry and physics. 81st ed. Boca Raton (FL): CRC Press.
- Mukhopadhyay S, Masto R, Tripathi R, Srivastava N. 2019. Chapter 14 application of soil quality indicators for the phytorestoration of mine spoil dumps. In: Pandey VC, Bauddh K, editors. Phytomanagement of polluted sites. Amsterdam, Netherlands: Elsevier, p. 361–388.
- Muller K, Stark K, Emel'yanenko VN, Varfolomeev MA, Zaitsau DH, Shoifet E, Schick C, Verevkin SP, Arlt W. 2015. Liquid organic hydrogen carriers: thermophysical and thermochemical studies of benzyl- and dibenzyl-toluene derivatives. Ind Eng Chem Res. 54(32):7967–7976. doi: 10.1021/acs.iecr.5b01840
- Müller K, Thiele S, Wasserscheid P. 2019. Evaluations of concepts for the integration of fuel cells in liquid organic hydrogen carrier systems. Energy Fuels. 33(10):10324–10330. doi: 10.1021/acs.energyfuels.9b01939
- Niermann M, Beckendorff A, Kaltschmitt M, Bonhoff K. 2019. Liquid organic hydrogen carrier (LOHC) assessment based on chemical and economic properties. Int J Hydrogen Energy. 44(13):6631–6654. doi: 10.1016/j.ijhydene.2019.
- Nishikawa H, Sasou H, Kurihara R, Nakamura S, Kano A, Tanaka K, Aoki T, Ogami Y. 2008. High fuel utilization operation of pure hydrogen fuel cells. Int J Hydrogen Energy. 33(21):6262–6269. doi: 10.1016/j.ijhydene.2008.07.
- Otto M, Chagoya KL, Blair RG, Hick SM, Kapat JS. 2022. Optimal hydrogen carrier: holistic evaluation of hydrogen storage and transportation concepts for power generation, aviation, and transportation. J Energy Storage. 55:105714. doi: 10.1016/j.est.2022.105714
- Peters R, Deja R, Engelbracht M, Frank M, Nguyen VN, Blum L, Stolten D. 2016. Efficiency analysis of a hydrogen-fueled solid oxide fuel cell system with anode off-gas recirculation. J Power Sources. 328:105–113. doi: 10.1016/j.jpowsour.2016.08.002
- Preuster P, Fang Q, Peters R, Deja R, Nguyen VN, Blum L, Stolten D, Wasserscheid P. 2018. Solid oxide fuel cell operating on liquid organic hydrogen carrier-based hydrogen making full use of heat integration potentials. Int J Hydrogen Energy. 43(3):1758–1768. doi: 10.1016/j.ijhydene.2017.11.054
- Rassat S, Aardahl C, Autrey T, Smith R. 2010. Thermal stability of ammonia borane: a case study for exothermic hydrogen storage materials. Energy & Fuels. 24(4):2596–2606. doi: 10.1021/ef901430a
- Rivard E, Trudeau M, Zaghib K. 2019. Hydrogen storage for mobility: a review. Materials. 12(12):1973. doi: 10.3390/ma12121973
- Rosado DM, Chavez SR, de Carvalho Jr J. 2019. Determination of global efficiency without/with supplementary burning of a thermoelectric plant with combined cycle of natural gas. In: 25th International Congress of Mechanical Engineering; Uberlandia, MG, Brazil; 10.
- Santos NP. 2022. Hydrogen in the portuguese navy: a case study. Int J Hydrogen Energy. 47(66):28684–28698. doi: 10.1016/j.ijhydene.2022.06.180
- Stark K, Emelyanenko VN, Zhabina AA, Varfolomeev MA, Verevkin SP, Müller K, Arlt W. 2015. Liquid organic hydrogen carriers: thermophysical and thermochemical studies of carbazole partly and fully hydrogenated derivatives. Ind Eng Chem Res. 54(32):7953–7966. doi: 10.1021/acs.iecr.5b01841
- Teichmann D, Stark K, Müller K, Zoettl G, Wasserscheid P, Arlt W. 2012. Energy storage in residential and commercial buildings via liquid organic hydrogen carriers (LOHC). Energy Environ Sci. 5(10):9044–9054. doi: 10.1039/c2ee22070a
- Tornatore C, Marchitto L, Sabia P, de Joannon M. 2022. Ammonia as green fuel in internal combustion engines: state-of-the-art and future perspectives. Front Mech Eng. 8:944201. doi: 10.3389/fmech.2022.944201
- Van Hoecke L, Laffineur L, Campe R, Perreault P, Verbruggen SW, Lenaerts S. 2021. Challenges in the use of hydrogen for maritime applications. Energy Environ Sci. 14(2):815–843. doi: 10.1039/D0EE01545H
- Van Rheenen E, Padding J, Kana A, Visser K. 2024. Ship system design changes for the transition to hydrogen carriers. In International Marine Design Conference; Amsterdam, The Netherlands. https://proceedings.open.tudelft.nl/imdc 24/article/view/894.
- Van Rheenen ES, Padding JT, Slootweg JC, Visser K. 2023. Hydrogen carriers for zero-emission ship propulsion using pem fuel cells: an evaluation. J Mar Eng Technol. 23(3):1–18.



- van Veldhuizen B, van Biert L, Amladi A, Woudstra T, Visser K, Aravind P. 2023. The effects of fuel type and cathode off-gas recirculation on combined heat and power generation of marine sofc systems. Energy Convers Manag. 276:116498. doi: 10.1016/j.enconman.2022.116498
- Wang X, Sun BG, Luo QH. 2019. Energy and exergy analysis of a turbocharged hydrogen internal combustion engine. Int J Hydrogen Energy. 44(11):5551–5563. doi: 10.1016/j.ijhydene.2018.10.047
- Wang Y, Pang Y, Xu H, Martinez A, Chen KS. 2022. Pem fuel cell and electrolysis cell technologies and hydrogen infrastructure development a review. Energy Environ Sci. 15(6):2288–2328. doi: 10.1039/D2EE00790H
- Wu M, Zheng Q, Sun T, Zhang X. 2023. Analysis of heat conducting enhancement measures on the composite for hydrogen storage by incorporation of activated carbon with mofs. Int J Hydrogen Energy. 48(10):3994–4005. doi: 10.1016/j.ijhydene.2022.10.245
- Yamada N, Mohamad MNA. 2010. Efficiency of hydrogen internal combustion engine combined with open steam rankine cycle recovering water and waste heat. Int J Hydrogen Energy. 35(3):1430–1442. doi: 10.1016/j.ijhydene.2009.11.088

- Yao J, Wu Z, Wang H, Yang F, Xuan J, Xing L, Ren J, Zhang Z. 2022. Design and multi-objective optimization of low-temperature proton exchange membrane fuel cells with efficient water recovery and high electrochemical performance. Appl Energy. 324:119667. doi: 10.1016/j.apenergy.2022.119667
- Ye L, Li D, Dong YP, Xu B, Zeng D. 2020. Measurement of specific heat capacity of NaBo₂(aq) solution and thermodynamic modeling of NaBO₂ + H₂O, NaBo₂ + NaCl + H₂O, and NaBO₂ + Na₂So₄ + H₂O systems. J Chem Eng Data. 65(5):2548–2557. doi: 10.1021/acs.jced.9b01182
- Zhang J, Fisher TS, Gore JP, Hazra D, Ramachandran PV. 2006. Heat of reaction measurements of sodium borohydride alcoholysis and hydrolysis. Int J Hydrogen Energy. 31(15):2292–2298. doi: 10.1016/j.ijhydene.2006.02.
- Zhao L, Brouwer J, James S, Siegler J, Peterson E, Kansal A, Liu J. 2017. Dynamic performance of an in-rack proton exchange membrane fuel cell battery system to power servers. Int J Hydrogen Energy. 42(15):10158–10174. doi: 10.1016/j.ijhydene.2017.03.004